ELSEVIER

Chemical Physics 270 (2001) 133–139

Chemical Physics

www.elsevier.com/locate/chemphys

The dynamics of oxygen atom formation in the UV photodissociation of nitromethane

Moon Soo Park [a], Kyung-Hoon Jung [a,*], Hari P. Upadhyaya [b], Hans-Robert Volpp [c]

[a] *Department of Chemistry and School of Molecular Science (BK21), Korea Advanced Institute of Science and Technology, Taeduck Science Town, Taejon 305-701, South Korea*

[b] *Chemistry Division, Bhabha Atomic Research Centre, Mumbai 400 085, India*

[c] *Physikalisch-Chemisches Institut der Universitat Heidelberg Im Neuenheimer Feld 253, D-69120 Heidelberg, Germany*

Received 27 January 2001

Abstract

The dynamics of oxygen atom formation in the gas-phase photolysis of nitromethane (CH_3NO_2) was studied using the pulsed laser photolysis/laser-induced fluorescence (LIF) pump-and-probe technique. Room-temperature CH_3NO_2 molecules were excited at two UV photodissociation laser wavelengths of 248 and 266 nm. Nascent $O(^3P)$ photofragments were detected via LIF in the vacuum ultraviolet spectral region under collision-free conditions. Narrow-band probe laser light, tunable over the wavelength range 130.2–130.6 nm, was used to monitor the fine-structure state distribution of nascent $O(^3P_{J=2,1,0})$ atom product. From Doppler profiles of the O atom, the fraction of the total available energy channeled into product translational energy was determined to be $\langle f_T \rangle = 0.28 \pm 0.02$ at 248 nm and $\langle f_T \rangle = 0.23 \pm 0.04$ at 266 nm. These f_T values are considerably lower than the value of $\langle f_T \rangle = 0.63$ obtained by dynamical simulation of the soft impulsive model for single N–O bond cleavage. The population ratio of the three fine-structure states of the oxygen atoms was found to be close to the statistical ratio at both photolysis wavelengths. The product fine-structure state population distribution measured for the O atoms and the $\langle f_T \rangle$ values indicate that at both photodissociation wavelengths the O atoms are produced mainly via an indirect predissociation mechanism, but at 248 nm there is an additional contribution from a direct predissociation mechanism. The absolute quantum yields for $O(^3P)$ atom formation were $\phi(O) = 0.18 \pm 0.03$ at 248 nm and $\phi(O) = 0.13 \pm 0.04$ at 266 nm; these values were obtained using a photolytic calibration method that employed NO_2 photodissociation as a reference source of well-defined O atom concentration. © 2001 Elsevier Science B.V. All rights reserved.

1. Introduction

The UV photoexcitation dynamics of nitromethane (CH_3NO_2) has attracted considerable attention among researchers owing to its complex primary photodissociation feature, which stands in contrast to the structural simplicity of nitromethane [1–17]. In particular, the competition among the various energetically allowed product decay channels makes it an interesting system for experimental and theoretical studies.

The CH_3NO_2 molecule exhibits two distinctly different UV absorption bands; a first strong band located at around 198 nm ($\varepsilon = 5000\ M^{-1}\,cm^{-1}$)

* Corresponding author. Fax: +82-42-869-8123.
E-mail address: khjung@mail.kaist.ac.kr (K.-H. Jung).

0301-0104/01/$ - see front matter © 2001 Elsevier Science B.V. All rights reserved.
PII: S0301-0104(01)00394-9

and a second much weaker one at approximately 270 nm ($\varepsilon = 10\ M^{-1}\,cm^{-1}$) [1,2]. In the wavelength region of the first band, the $\pi^* \leftarrow$ n transition is localized on the NO_2 moiety and the main photodissociation channel is found to be $CH_3NO_2 \rightarrow CH_3 + NO_2$, which occurs via electronic and vibrational predissociations [3–6]. Nevertheless, $\pi^* \leftarrow$ n excitation of a nonbonding electron of the O atom is also responsible for at least three additional photodissociation channels, including a channel that leads to NO and O atom formation [7–9]. Past studies of NO_2 formation dynamics by femtosecond laser-induced fluorescence (LIF) at 266 nm have yielded conflicting results for the product quantum yield; for example Shoen et al. [8] give a value of $\Phi = 0.7$, whereas Mialocq et al. [9] state the value at $\Phi = 0.17$.

In this article we report on the O atom formation dynamics photolysis of CH_3NO_2 at 248 and 266 nm, studied using the pulsed laser photolysis (LP/VUV) LIF pump-and-probe method. The product quantum yield for oxygen atom formation was determined by a photolytic calibration method using a NO_2 reference gas. Finally, we attempt to clarify the unresolved discrepancy between past results by proposing a mechanism for O atom formation based on the observed $O(^3P_J)$ atom Doppler profiles and the nascent population distribution of three product fine-structure states of oxygen atom, i.e., $O(^3P_J; J = 0, 1, 2)$.

2. Experimental

The experimental setup used in this study was essentially the same as the flow system described in detail elsewhere [18]. A small modification was made to the LP/VUV-LIF pump–probe setup to allow for VUV-LIF detection of $O(^3P_J)$ atoms. CH_3NO_2 (Aldrich, purity > 99%) was flowed through the reactor at about 1–40 mTorr and constantly monitored by a pressure gauge (MKS-Baratron). The system was at room temperature, and the flow rate was controlled using a calibrated mass flow controller. The calibration was done with NO_2 (Messer Greisheim, 99.98%) gas at a pressure of approximately 40 mTorr. The flow rate of reactants was maintained at a level sufficient to ensure fresh sample gases at each of the successive laser shots made at a repetition rate of 6 Hz.

Photolyses of CH_3NO_2 and NO_2 were performed at 248 nm using a KrF excimer laser and at 266 nm using the fourth harmonic of a Nd/YAG laser. The homogeneous part of the rectangular excimer laser profile was skimmed off using a circular aperture to provide the photolysis beam. The photolysis laser intensities were typically 2–10 mJ/cm^2. Since the beam was essentially unpolarized, any anisotropy in the photodissociation process was expected to be largely averaged out. To detect $O(^3P_J)$ atoms narrow-band probe laser light in the wavelength region 130.21–130.60 nm was generated using Wallenstein's method [19] for the resonance third-order sum–difference frequency conversion ($\omega_{VUV} = 2\omega_R - \omega_T$) of pulsed dye laser light in Kr gas. The fixed frequency ω_R (212.55 nm) was the two-photon resonance of the Kr transition 4p–5p (1/2, 0), and the frequency ω_T was tuned from 570 to 579 nm. The "primary" laser light for the nonlinear mixing process was obtained from two tunable dye lasers simultaneously pumped by a XeCl excimer laser, one of which, ω_R, was frequency doubled using a BBO II crystal. The VUV-light generated in the four-wave mixing process was carefully separated from the unconverted laser light by a lens monochromator followed by a light baffle system. The bandwidth of the VUV light was determined to be 0.43 ± 0.04 cm^{-1} through analysis of the O atom Doppler profiles measured under thermalized conditions, in the presence of a large excess of N_2.

The photolysis laser beam was aligned so as to overlap the probe beam at a right angle in the viewing region of the LIF detector. The delay time between the pump pulse (duration $\approx$ 10 ns) and probe pulse (duration $\approx$ 15 ns) lasers was typically 150 ± 10 ns. This delay was sufficient to avoid any time overlap between these pulses and any unwanted multiphoton photochemical processes. The LIF signal was passed through a band-pass filter and measured with using a solar blind photomultiplier positioned at right angles to both laser beams. The S/N ratio was determined by averaging each point of the O atom Doppler profiles over 30 laser shots. The fluctuation in intensity of the VUV probe laser beam was monitored using an addi-

tional solar blind photomultiplier of the same type. The O atom LIF signal and the intensities of the probe and photolysis laser beam intensities were recorded using a three-channel boxcar system and transferred to a microcomputer via an analogue-to-digital converter. The LIF signal was normalized both photolysis and probe laser intensities. Log–log plots of O signal intensity against photolysis laser intensities at 248 and 266 nm were linear, with slopes of 0.83 ± 0.08 and 0.81 ± 0.11, respectively.

3. Results

3.1. $O(^3P)$ fine-structure state distribution

Fig. 1 shows typical Doppler profiles of $O(^3P_J; J = 2, 1, 0)$ atoms produced in the gas-phase dissociation of room-temperature CH_3NO_2 after excitation at 248 nm. The fine-structure state distribution of $O(^3P_J; J = 2, 1, 0)$ fragments was determined from the integrated areas of the Doppler profiles, after correcting for slight fluctuations in the oscillator strengths of the spectral transitions used for probing different J-states.

3.2. Average O atom translational energy

The LIF of $O(^3P_J)$ atoms was observed by employing $^3S_1 \leftarrow {}^3P_J$ transitions in the 130.21–130.60 nm region. O atom Doppler profiles were measured to obtain the fraction of the average available energy, $\langle f_T \rangle$, released as translational energy after photoexcitation of CH_3NO_2 at 248 and 266 nm. The average translational energy of the product in a center-of-mass system was calculated from the FWHM of the profile obtained by fitting a Gaussian function to the observed O atom Doppler profile. The average translational energies, $E_{T(c.m)}$, for the $CH_3NO + O$ channel at 248 and 266 nm were found to be 25.1 ± 1.9 and 13.6 ± 2.1 kJ/mol, respectively. The energies available to the products were obtained from the photon energies used in photolysis and from available thermochemical data [20,21]. The $\langle f_T \rangle$ values thus determined were 0.28 ± 0.02 at 248 nm and 0.23 ± 0.04 at 266 nm. The $\langle f_T \rangle_{IM}$ value was calculated to be 0.63 using a soft impulsive model defined in Eqs. (1) and (2), where μ is the reduced mass, and E_{avl} is the available energy.

$$E_{T,IM} = \frac{\mu_{N\text{–}O}}{\mu_{CH_3NO\text{–}O}}(h\nu - D_0) = \frac{\mu_{N\text{–}O}}{\mu_{CH_3NO\text{–}O}}E_{avl} \quad (1)$$

$$\langle f_T \rangle_{IM} = \frac{E_{T,IM}}{E_{avl}} = \frac{\mu_{N\text{–}O}}{\mu_{CH_3NO\text{–}O}} \quad (2)$$

Comparison of the experimental values with the values of $\langle f_T \rangle_{IM}$ from the soft impulsive model indicates that the available energy in the photodissociation process is partitioned in a nearly statistical fashion (see Table 1).

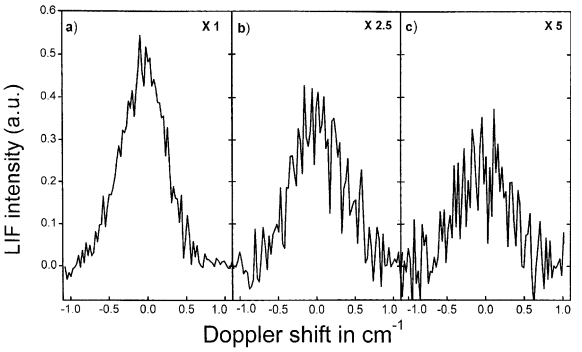

Fig. 1. Doppler profiles of $O(^3P_J)$ atoms for: (a) $J = 2$, (b) $J = 1$ and (c) $J = 0$ produced in the 248 nm photolysis of nitromethane. Line centers correspond to the $^3S_1 \leftarrow {}^3P_J$ transition of the O atom at (a) 76 794.69 cm^{-1}, (b) 76 636.19 cm^{-1} and (c) 76 568.19 cm^{-1}.

3.3. Nascent $O(^3P_J)$ fine-structure state distributions

The $O(^3P_J)$ atom quantum yields were obtained by a calibration method using NO_2 as a reference.

Table 1
The fraction of available energy released into product translational energy in the center-of-mass frame of the $CH_3NO + O$ products

Photolysis wavelength (nm)	$E_{c.m}$(kJ/mol)	$\langle f_T \rangle$	$\langle f_T \rangle_{Im}$ [a]
248	25.1 ± 1.9	0.28 ± 0.02	0.63
266	13.6 ± 2.1	0.23 ± 0.04	0.63

[a] Calculated employing a soft impulsive model.

The measured ratio of $\Phi_{NO_2}(O(^3P_2)):\Phi_{NO_2}(O(^3P_1)):\Phi_{NO_2}(O(^3P_0))$ at 266 nm agreed well with the literature value [22,23]. Our measured ratio of $\Phi_{NO_2}(O(^3P_2)):\Phi_{NO_2}(O(^3P_1)):\Phi_{NO_2}(O(^3P_0))$ at 248 nm was almost the same as that at 266 nm.

$$\Phi_{CH_3NO_2}(O(^3P_J)) = \gamma_O \frac{S_O(CH_3NO_2)\Phi_{NO_2}(O(^3P_J))\sigma_{NO_2}P_{NO_2}}{S_O(NO_2)\sigma_{CH_2NO_2}P_{CH_3NO_2}} \quad (3)$$

$$\Phi_{NO_2}(O) = \Phi_{NO_2}(O(^3P_2)) + \Phi_{NO_2}(O(^3P_1)) + \Phi_{NO_2}(O(^3P_0)) \approx 1 \quad (4)$$

$$\Phi_{CH_3NO_2}(O) = \Phi_{CH_3NO_2}(O(^3P_2)) + \Phi_{CH_3NO_2}(O(^3P_1)) + \Phi_{CH_3NO_2}(O(^3P_0)) \quad (5)$$

The ratios of $\Phi_{CH_3NO_2}(O(^3P_2)):\Phi_{CH_3NO_2}(O(^3P_1)):\Phi_{CH_3NO_2}(O(^3P_0))$ in Eq. (3) were found to be 75:19:6 at 248 nm and 73:20:7 at 266 nm (Table 2). The total quantum yield $\Phi_{CH_3NO_2}(O)$ for the $(CH_3NO + O)$ channel was also determined from Eqs. (4) and (5) and was found to be $(17.8 \pm 3.3)\%$ at 248 nm and $(13.1 \pm 3.7)\%$ at 266 nm, where S_O is the integrated area under the measured $O(^3P_J)$ atom Doppler profile. The parameters σ_{NO_2} and $\sigma_{CH_3NO_2}$ are the absorption cross-sections of NO_2 and CH_3NO_2, respectively. P_{NO_2} and $P_{CH_3NO_2}$ are the pressures of NO_2 and CH_3NO_2. The parameter γ_O is a constant obtained experimentally. The values of $\sigma_{CH_3NO_2}$ measured in this study were $(1.17 \pm 0.05) \times 10^{-19}$ at 248 nm and $(1.24 \pm 0.05) \times 10^{-19}$ cm^2 at 266 nm. The values used for σ_{NO_2} were 3.2×10^{-20} and 3.0×10^{-20} cm^2, as obtained from Ref. [24].

Table 2
Primary photolytic oxygen atom quantum yield $\Phi(O)$ and the nascent population ratios of the $O(^3P_J)$ fine-structure states in the CH_3NO_2 photolysis

Photolysis wavelength (nm)	$\Phi(O)$	$N(O(^3P_2))/N(O(^3P_1))/N(O(^3P_0))$
248	0.18 ± 0.03	0.75/0.19/0.06
266	0.13 ± 0.04	0.73/0.20/0.07

4. Discussion

4.1. Quantum yields of photodissociation channels in the $\pi^* \leftarrow n$ transition

Three important channels in R-NO_2 photolysis are summarized by [3–9,13]

$$RNO_2 + h\nu \rightarrow R + NO_2 \text{ (C–N cleavage)} \quad (a)$$

$$RNO_2 + h\nu \rightarrow RNO + O \text{ (N–O cleavage)} \quad (b)$$

$$RNO_2 + h\nu \rightarrow RO + NO \text{ (N–O cleavage after isomerization)} \quad (c)$$

The contributions of these reaction channels vary from reaction to reaction. For instance, all three channels are involved in the case of $C_6H_5NO_2$ photolysis near 248 nm. Our measured quantum yield is 0.39 ± 0.08 in channel (b). For CH_2NO_2, channels (b) and (c) are the major photolysis channels in the region of 240–270 nm [11]. In the case of CH_3NO_2, the major contribution in the $\pi^* \leftarrow \pi$ transition has been found to be channel (a) with nearly unit quantum yield [3–5], but the detailed mechanism in the $\pi^* \leftarrow n$ transition has yet to be studied [8,9]. In the present study, the total dissociation behavior of CH_3NO_2 in the $\pi^* \leftarrow n$ transition is explored in some detail.

The total quantum yield of the dissociation channels is assumed to be one, because CH_3NO_2 gives out negligible fluorescence in the $\pi^* \leftarrow n$ transition [25]. In 266-nm photolysis, the ground state $NO_2(^2A_1)$ and a very small amount of the excited state NO_2^* were formed from the $(CH_3 + NO_2)$ channel. Ab initio calculation [12] has shown that the ground state $NO_2(^2A_1)$ is related to the ground potential energy surface ($^1A_1$). These results imply that the $(CH_3 + NO_2(^2A_1))$ channel in the $\pi^* \leftarrow n$ transition proceeds by indirect predissociation transferring from the first excited state ($^1A_2$) to the ground state ($^1A_1$). An infrared multiphoton dissociation (IRMPD) study has suggested competition between the $(CH_3O + NO)$ channel and the $(CH_3 + NO_2(^2A_1))$ channel on the ground PES of CH_3NO_2 [15,16]. The A factors of channels (a) and (c) have been reported, at $10^{15.6}$ and $10^{13.3}$, respectively [15,16]. Since nitromethane

obtains sufficient energy to cross the energy barriers (251.9 kJ/mol for channel (a) and 231.6 kJ/mol for channel (c)), the relative yield between channels (a) and (c) can be estimated from the A factors of these channels. Given that the A factor of channel (a) is ten times larger than that of channel (c), it is reasonable to assume that the yield of channel (a) will be considerably larger than that of channel (c). Since channel (b) is also involved in indirect predissociation in the ground PES, these three channels must compete on the ground PES of CH_3NO_2 photolysis by $\pi^* \leftarrow$ n transition.

Although several minor dissociation channels are also energetically feasible, their contributions seem to be very small. For instance, the observed quantum yield of the channel ($CH_2NO + OH$) is only 0.004 ± 0.001 [17]. Another possible channel, ($CH_2NO_2 + H$), requires C–H bond fission after energy transfer from the NO_2 moiety. It has not yet been confirmed whether or not another possible channel, ($CH_2O + HNO$), is a primary reaction [7]. The ($C_2H_4 + HONO$) channel for decomposition of nitroethane via an intramolecular rearrangement has been suggested, but HONO formation has yet to be observed experimentally [26] (see Table 3).

Accepting $\Phi = 0.13$ at 266 nm for channel (b), it is reasonable to adopt $\Phi_{CH_3+NO_2} = 0.7 \pm 0.3$ for channel (a) at 266 nm. In order to confirm the proposed mechanism for the photodissociation of CH_3NO_2 after $\pi^* \leftarrow$ n excitation, the quantum yield for the product channel (c) has to be measured.

4.2. The oxygen atom formation mechanism of CH_3NO_2

The LIF profiles of $O(^3P_2)$ atoms in Fig. 2 are well fitted with a Gaussian functions which indicate that O atoms are produced through slow processes, for example by indirect predissociation through the internal conversion between an excited state PES and the ground state PES, followed by direct predissociation by crossing between two excited state PESs. The observation of almost equal ratios of $O(^3P_J)$ at 248 and 266 nm suggests that the $CH_3NO + O$ reaction occur via very similar dissociation mechanisms at the two wavelengths. The fraction of the average available energy released as translational energy is much smaller than the fraction calculated using the soft impulsive model (see Table 1). This implies that the dissociation time is long enough for the available energy to be released into internal energy.

The larger value of $\langle f_T \rangle$ at 248 nm ($\langle f_T \rangle = 0.28$) than at 266 nm ($\langle f_T \rangle = 0.23$) suggests that direct predissociation participates in the ($CH_3NO + O$) channel at 248 nm, because more of the available energy is released to translational energy than that would be expected for indirect predissociation. Although the Doppler profile of $O(^3P_2)$ at 248 nm is well fitted by a Gaussian function, the relatively large laser bandwidth and error range make it difficult to determine whether one or two dissociation channels are involved. The origin of the large value of $\langle f_T \rangle$ at 248 nm can be found in the dynamics of the ($CH_3 + NO_2$) channel [8,12]. The ratio of $NO_2^*(1^2B_2)$ and $NO_2(1^2A_2)$ at 248 nm in

Table 3
Quantum yields of the primary product channels in the dissociation of CH_3NO_2 after $\pi^* \leftarrow$ n photoexcitation

Product channel	Quantum yield	ΔH_0 (eV)	Mechanism	Experimental technique
$CH_3 + NO_2$	0.70 ± 0.30[a]	1.87	C–N cleavage	LIF [4]
$CH_3 + NO + O$	0.13 ± 0.08[b]	4.07	N–O cleavage	LIF
$CH_3O + NO$	–[c]	1.7	Isomerization + N–O cleavage	IRMPD [15,16]
$CH_2 + NO + OH$	0.004 ± 0.001	2.61	Isomerization + elimination	LIF [17]
$CH_2 + NO_2 + H$	–[d]	3.92	C–H cleavage	Flash photolysis [7]
$CH_2 + HONO$	–[d]	2.78	Isomerization + elimination	Flash photolysis [25]
$CH_2O + HNO$	–[d]	0.68	Isomerization + elimination	Flash photolysis [7]

[a] Quantum yield at 266 nm.
[b] This work.
[c] Unknown, but expected to be considerably less than the quantum yield of the $CH_3 + NO_2$ product channel.
[d] Unknown, but expected to be very small.

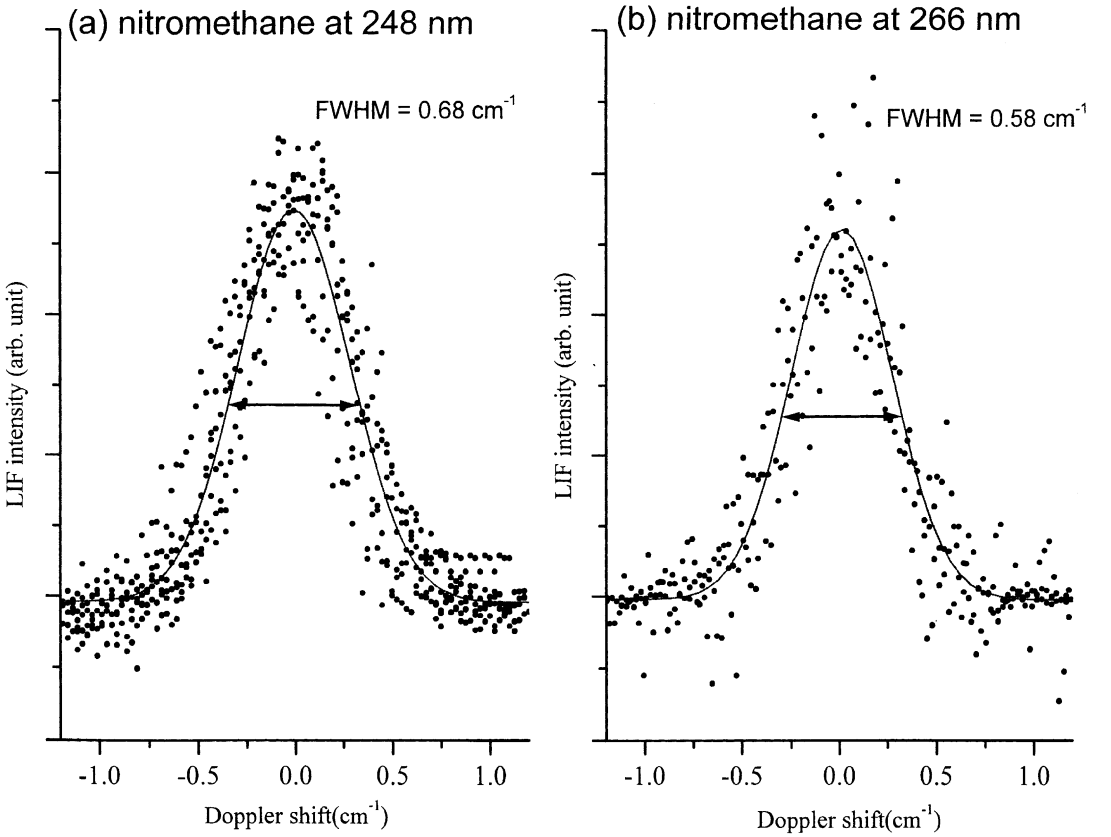

Fig. 2. Doppler profiles of $O(^3P_2)$ atoms produced: (a) at 248 nm and (b) at 266 nm in the photolysis of nitromethane. Line centers correspond to the $^3S_1 \leftarrow {}^3P_2$ transition of the O atom (76 794.69 cm^{-1}).

the CH_3NO_2 photolysis was found to be smaller than that at 266 nm, and considerably larger than that at 240 nm. $NO_2^*(1^2B_2)$ comes from the $^1B_2(n\sigma^*)$ repulsive PES [12], and only the $^1A_2$ excited state is accessible via a one-photon absorption transition at 240 and 266 nm [10]. Although the $^1B_2(n\sigma^*)$ repulsive PES has no correlation with the $^1A_2$ excited state PES in C_{2v} symmetry, the crossing from the $^1B_2(n\sigma^*)(A')$ PES to the $^1A_2(A')$ excited state PES is accessible with breaking of the C_{2v} symmetry by symmetric vibration of CH_3NO_2. This may be the origin of the direct predissociation which produces $NO_2(1^2B_2)$. The crossing point is located at between 37 593 cm^{-1} (266 nm) and 41 667 cm^{-1} (240 nm). Assuming an unknown repulsive PES related to $(CH_3NO(^3A'') + O(^3P_J))$, the coupling with the $^1A_2$ excited state PES by the C_{2v} symmetry breaking to C_1 would explain the larger $\langle f_T \rangle$ at 248 nm than at 266 nm in the $(CH_3NO + O)$ channel. The crossing point may be in the range of 37 593 cm^{-1} (266 nm) to 40 323 cm^{-1} (248 nm). This reasoning, would explain why O atoms are produced via indirect predissociation only at 266 nm, and via direct and indirect predissociation at 248 nm in the $\pi^* \leftarrow$ n transition of the CH_3NO_2 system.

We have proposed that the CH_3NO_2 dissociation process at 248 nm involves competition between an indirect and a direct predissociation. $NO_2^*(1^2B_2)$ and O atoms are expected to be the main products from predissociation. From the absolute quantum yields for $O(^3P)$ at 248 and 266 nm, we have confirmed channel (a) is the main channel with its quantum yield of about 0.7.

Acknowledgements

The authors gratefully acknowledge the financial support of the Korea Science and Engineering Foundation for the Korea–Germany Joint Research Project 1999-2001. HPU also wishes to acknowledge a fellowship provided by the DLR Bonn under Indo-German bilateral agreement, project no. INI-207.

References

[1] W.D. Taylor, T.D. Allston, M.J. Moscato, G.B. Fazekas, R. Kozlowski, G.A. Takacs, Int. J. Chem. Kinet. 12 (1980) 231.
[2] S. Nagakura, Mol. Phys. 3 (1960) 152.
[3] N.C. Blais, J. Chem. Phys. 79 (1983) 1723.
[4] L.J. Butler, D. Krajnovich, Y.T. Lee, J. Chem. Phys. 79 (1983) 1708.
[5] D.B. Moss, K.A. Trentelman, P.L. Houston, J. Chem. Phys. 96 (1992) 237.
[6] K.Q. Lao, E. Jensen, P.W. Kash, L.J. Butler, J. Chem. Phys. 93 (1990) 3958.
[7] K. Honda, H. Mikuni, M. Takahasi, Bull. Chem. Soc. Jpn. 45 (1972) 3534.
[8] P.E. Shoen, M.J. Marrone, J.M. Schnur, L.S. Goldberg, Chem. Phys. Lett. 90 (1982) 272.
[9] J.C. Mialocq, J.C. Stephenson, Chem. Phys. 106 (1986) 281.
[10] L.E. Harris, J. Chem. Phys. 58 (1973) 5615.
[11] D.R. Cyr, D.J. Osborn, R.E. Continetti, D.M. Neumark, J. Chem. Phys. 99 (1993) 8751.
[12] C. Mijoule, S. Odiot, S. Fliszar, J.M. Schnur, J. Mol. Struct. (Theochem) 149 (1987) 311.
[13] H.S. Kilic, K.W.D. Ledingham, C. Kosmidis, T. McCanny, R.P. Singhal, S.L. Wang, D.J. Smith, A.J. Langley, W. Shaikh, J. Phys. Chem. A 101 (1997) 817.
[14] K.G. Spears, S.P. Brugge, Chem. Phys. Lett. 54 (1978) 373.
[15] A.M. Wodtke, E.J. Hintsa, Y.T. Lee, J. Chem. Phys. 84 (1986) 1044.
[16] A.M. Wodtke, E.J. Hintsa, Y.T. Lee, J. Phys. Chem. 90 (1986) 3549.
[17] S. Zabarnick, J.W. Fleming, A.P. Baronavski, J. Chem. Phys. 85 (1986) 3395.
[18] R.A. Brownsword, M. Hillrenkamp, T. Laurent, R.K. Vatsa, H.R. Volpp, J. Wolfrum, J. Phys. Chem. A 101 (1997) 995.
[19] G. Hilber, A. Lago, R. Wallenstein, J. Opt. Soc. Am. B 4 (1987) 1753.
[20] S.W. Benson, Thermochemical Kinetics, second ed. Wiley, New York, 1976.
[21] C.F. Melius, BAC-MP4 ab initio calculation.
[22] J. Miyawaki, T. Tsuchizawa, K. Yamanouchi, S. Tsuchiya, Chem. Phys. Lett. 165 (1990) 168.
[23] H.G. Rubahn, W.J. van der Zande, R. Zhand, M.J. Bronikowski, R.N. Zare, Chem. Phys. Lett. 186 (1991) 154.
[24] D.L. Baulch, C.J. Cobos, R.A. Cox, C. Esser, P. Frank, Th. Just, J.A. Kerr, M.J. Pilling, J. Troe, R.W. Walker, J. Warnatz, J. Phys. Chem. Ref. Data 21 (1992) 411.
[25] S. Nagakura, M. Kojima, Y. Maruyama, J. Mol. Spectrosc. 13 (1964) 174.
[26] R.E. Rebbert, N. Slagg, Bull. Soc. Chim. Belges. 72 (1962) 709.